Black Sea Journal of Engineering and Science
doi: 10.34248/bsengineering.1776780

Open Access Journal
e-ISSN: 2619 – 8991

Research Article
Volume 9 - Issue 1: 192-205 / January 2026

SYNTHESIS, SPECTROSCOPIC AND THEORETICAL CHARACTERIZATION OF CHIRAL BENZIMIDAZOLE-BASED SCHIFF BASES

Nuriye Tuna SUBAŞI[1*]

[1]*Kırşehir Ahi Evran University, Faculty of Engineering and Architecture, Department of Food Engineering, 40100, Kırşehir, Türkiye*

Abstract: Schiff bases are versatile compounds widely utilized in organic chemistry, serving as essential intermediates, starting materials, ligands, and catalysts. Their increasing significance in both practical applications and biological studies, particularly the notable bioactivity of their transition metal complexes, has sparked extensive scientific interest. In this context, the present study focuses on synthesizing novel chiral Schiff bases derived from benzimidazole, utilizing natural chiral amino acids as starting points. The condensation of these precursors with 4-(dimethylamino)benzaldehyde yielded four new Schiff base derivatives. To further investigate their potential biological activity, molecular docking studies were performed to examine the binding interactions between the synthesized compounds and selected target proteins. The results indicated that some derivatives showed high binding affinity, implying potential inhibitory activity. These findings highlight the promising pharmacological relevance of the synthesized compounds and support their future exploration in drug discovery research. Moreover, their coordination ability suggests potential applications as ligands in transition metal complexation.

Keywords: Benzimidazole, Schiff base, Molecular docking, Biological activity

***Corresponding author:** Kırşehir Ahi Evran University, Faculty of Engineering and Architecture, Department of Food Engineering, 40100, Kırşehir, Türkiye
E mail: nsubasi@ahievran.edu.tr (N.T. SUBAŞI)
Nuriye Tuna SUBAŞI https://orcid.org/0009-0005-2122-0402

Received: September 02, 2025
Accepted: November 16, 2025
Published: January 15, 2026

Cite as: Subaşı, N. T. (2026). Synthesis, spectroscopic and theoretical characterization of chiral benzimidazole-based Schiff bases. *Black Sea Journal of Engineering Science, 9*(1), 192–205.

1. Introduction

Schiff bases are compounds formed as a result of a nucleophilic addition reaction between aldehydes or ketones and primary amines under appropriate conditions. These compounds are characterized by a carbon-nitrogen double bond (–CH=N–) in their structure, as shown in Figure 1. The discovery of Schiff bases dates back to 1864 (Schiff, 1869), when Hugo Schiff first reported the formation of imine-based compounds. Their potential as ligands in coordination chemistry was later recognized, particularly through the work of Pfeiffer and colleagues in the early 1930s (Pfeiffer et al., 1932). With the advancement of spectroscopic techniques, the roles of these compounds in biochemical processes have been more thoroughly investigated. Studies have shown that these compounds can participate in various biochemical processes by interacting with free metal ions and reducing the reactivity of aldehyde and amine groups, thereby minimizing their potential toxicity.

Thanks to their rigid molecular structures, synthetic flexibility, and ease of derivatization, Schiff bases have become essential scaffolds in various branches of modern chemistry. Their coordination abilities enable the formation of highly stable metal complexes, which exhibit a wide range of biological effects, including anticancer, antimicrobial, antiviral, herbicidal, antifungal and antioxidant activities (Rehman et al., 2004; Golcu et al., 2005; Ashraf et al., 2011; Silva da et al., 2011). Moreover, these compounds serve in diverse roles such as corrosion inhibitors (Emregül et al., 2006), ion carriers (Aydınlı, 2006), catalysts (Redshaw, 2017), analytical reagents, and in advanced technological applications (Upadhyay et al., 2008; DiRisio et al., 2017).

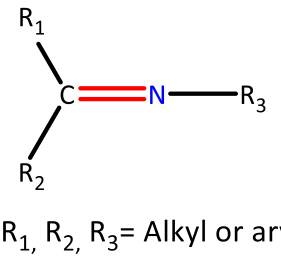

Figure 1. Representative structure of a Schiff base compound.

The versatility of Schiff bases arises from key features such as (Vigato and Tamburini, 2004): 1). Their ability to form via multiple synthetic strategies, especially through template methods. 2) The presence of donor atoms like nitrogen, oxygen, sulfur, and phosphorus that facilitate

coordination with a broad spectrum of metal ions. 3) Their modular structure, which permits functionalization through appropriate substituents. 4) Upon reduction, they can yield flexible polyamine derivatives that are less prone to hydrolysis. 5) They can be immobilized on surfaces like silica to develop heterogeneous catalysts. 6) When incorporated into macrocyclic systems, they provide selective metal-binding frameworks. 7) Their metal chelates can interact with DNA, enabling their use in the design of diagnostic and therapeutic agents.

Owing to their photoresponsive behavior, Schiff bases have also found application in the development of optoelectronic components, radiation detectors, and imaging systems (Yeap et al., 2003). Their colorful metal complexes make them valuable in the dye industry, especially as pigments in textile applications (Zeishen et al., 1990; Lasri et al. 2018). Moreover, they possess significant potential in perfumery, pharmaceutical industries, and oxygen transport systems. In analytical chemistry, their selective color changes in response to specific metal ions enable their use as spectrophotometric reagents. Furthermore, some Schiff base metal complexes exhibit liquid crystal properties, making them applicable in the development of aircraft materials, television and computer displays, and digital watch screens (Zhang et al., 2018).

A review of the current literature reveals that most synthesized Schiff bases are derived from salicylaldehyde and its derivatives, while Schiff bases based on benzimidazole derivatives have been reported less frequently. Benzimidazole is an aromatic heterocyclic compound consisting of an imidazole ring fused to a benzene ring and contains two nitrogen atoms. One of the best-known examples is N-ribosyl-dimethylbenzimidazole, which serves as a cobalt-binding ligand in vitamin B_{12} (Asif, 2019). The benzimidazole moiety constitutes the core structure of numerous therapeutic agents. For instance, omeprazole (anti-ulcer), bendamustine (anticancer), telmisartan (antihypertensive), and pimozide (antipsychotic) all contain a benzimidazole backbone (Chang, 2012; Iwamoto et al., 2017; Zhang et al., 2017; Lieberman and Higgins, 2009).

In this study, chiral benzimidazole derivatives were successfully synthesized starting from biologically significant amino acids. The use of amino acids as starting materials offers biocompatibility and potential biological activity to the synthesized compounds. Owing to their imidazole ring and stereocenters, the synthesized chiral benzimidazole derivatives are expected to possess pharmacological potential and the ability to interact with specific biological targets. These derivatives were subjected to condensation reactions with the electron-rich 4-(dimethylamino)benzaldehyde, yielding four novel Schiff bases. The structures of the obtained compounds were characterized by NMR spectroscopy and supported by theoretical calculations. Furthermore, to complement the experimental data, molecular docking simulations were conducted using the 2WQY protein structure, providing insights into the potential of these compounds as theoretical inhibitor candidates.

2. Materials and Methods

2.1. Materials

All chemical materials were obtained from commercial sources, including Sigma-Aldrich and Merck, and were used without any additional purification. Thin-layer chromatography (TLC) was carried out on silica-coated plates with aluminum backing (Merck silica gel 60 F_{254}), and the developed spots were visualized under UV light at a wavelength of 254 nm. For column chromatography, silica gel 60 with a particle size range of 40–63 μm was employed. NMR spectra were recorded on both Varian VNMRJ 400 and Bruker Avance 400 spectrometers, operating at 400 MHz, with DMSO-d_6 used as the deuterated solvent. Chemical shift values (δ) are given in parts per million (ppm) relative to internal references: for ^{1}H NMR, the residual peak of DMSO-d_6 at δ = 2.50 ppm, and for ^{13}C NMR, the corresponding signal at δ = 39.5 ppm.

2.2. Methods

2.2.1. Experimental studies

Within the scope of this study, four chiral Schiff bases containing benzimidazole moieties were successfully synthesized and characterized. In the first step, chiral benzimidazole derivatives (3a–3d) were synthesized by the condensation of 1,2-diaminobenzene (1) with amino acids S-valine, S-alanine, S-phenylalanine, and S-leucine (2a–2d), respectively. In the second step, each of the synthesized chiral benzimidazole derivatives was reacted with 4-(dimethylamino)benzaldehyde (4) to afford four new Schiff bases (5a–5d). The general synthetic route for the obtained compounds is illustrated in Figure 2.

2.2.1.1. Synthesis of chiral benzimidazole derivatives

An equimolar amount of o-phenylenediamine was stirred in 10-15 mL of 6 N hydrochloric acid at ambient temperature for approximately 10 minutes. Subsequently, 1.5 equivalents of the corresponding amino acid were introduced into the solution, and the reaction mixture was subjected to reflux conditions for a period of 72 hours. The course of the reaction was monitored via thin-layer chromatography (TLC). Once complete, the pH of the mixture was carefully adjusted to a range of 7-8 by the gradual addition of 20% aqueous ammonia, with pH confirmation performed using indicator paper. The resulting mixture was extracted with ethyl acetate, and the organic phase was collected, dried over anhydrous Na_2SO_4, and the solvent was evaporated under reduced pressure. The crude product was purified by column chromatography.

2.2.1.2. Synthesis of schiff bases

Equimolar amounts of the synthesized benzimidazole derivatives (3a-3d) were combined with 1.2 equivalents of 4-(dimethylamino)benzaldehyde in 20 mL of ethanol. To catalyze the reaction, a few drops of glacial acetic acid were introduced, and the mixture was subjected to reflux

for 12 hours. Upon completion, the reaction medium was transferred into ice-cold water to induce precipitation. The resulting solid was isolated by vacuum filtration and subsequently purified through recrystallization using ethanol as the solvent.

2.2.2. Theoretical Studies

In this study, theoretical calculations were performed using the Gaussian 09 software package (Frisch et al., 2009). This program allows for the computation of various molecular properties such as electronic energies, structural parameters, vibrational frequencies related to energy, force constants, dipole moments, thermochemical parameters, electron affinities, and ionization energies. The calculations were carried out using Density Functional Theory (DFT) with the B3LYP functional (Becke, 1993; Lee et al., 1988) and the 6-311G(d) basis set (Foresman and Frisch, 1996). For the graphical visualization and analysis of Gaussian output files, GaussView 5 software (Dennington et al., 2009) was utilized. For molecular docking simulations, the PyRx software (Dallakyan and Olson, 2015) was employed.

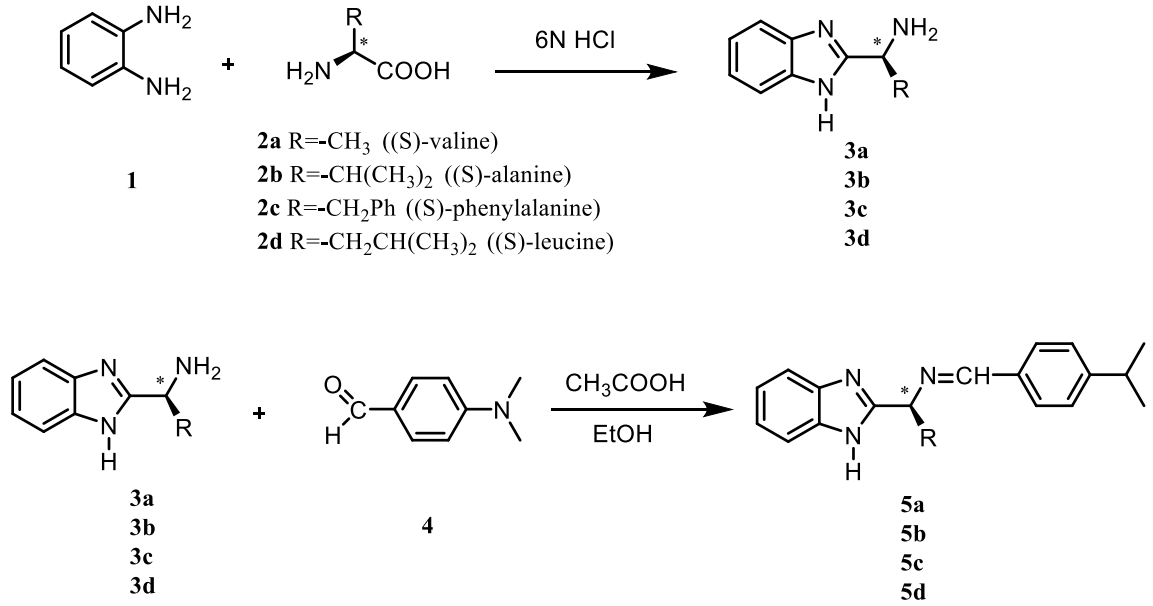

Figure 2. General synthesis of Schiff bases 5a–5d.

3. Results

(3a) 1-(1H-benzo[d]imidazol-2-yl)-2-methylpropan-1-amine

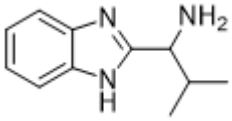

^{1}H NMR (400 MHz, DMSO-d_6): δ 7.62 (m, 2H, Ar–H), 7.16 (m, 2H, Ar–H), 4.21 (t, 1H, –CH–NH_2), 2.30 (m, 1H, –$CH(CH_3)_2$), 0.97 (d, J = 6.7 Hz, 6H, –CH_3). ^{13}C NMR (100 MHz, DMSO-d_6): δ 143.7, 138.9, 122.8, 114.8, 61.8, 35.4, 19.2.

(3b)1-(1H-benzo[d]imidazol-2-yl)ethan-1-amine

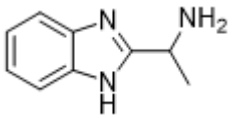

^{1}H NMR (400 MHz, DMSO-d_6): δ 7.51 (m, 2H, Ar-H), 7.15 (m, 2H, Ar-H), 4.41 (q, J = 6.9 Hz, 1H, –CH), 1.55 (d, J = 6.9 Hz, 3H, –CH_3). ^{13}C NMR (100 MHz, DMSO-d_6): δ 141.2, 139.2, 123.2, 116.6, 52.3, 24.4.

(3c) 1-(1H-benzo[d]imidazol-2-yl)-2-phenylethan-1-amine

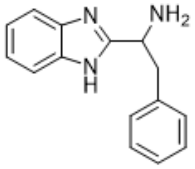

^{1}H NMR (400 MHz, DMSO-d_6): δ 7.53–7.24 (m, 4H, Ar–H), 7.23–7.16 (m, 5H, Ar–H), 5.25 (m, 1H, –CH), 3.51–3.35 (m, 2H, –CH_2). ^{13}C NMR (100 MHz, DMSO-d_6): δ 142.5, 139.2, 135.4, 131.0, 129.1, 127.6, 123.7, 119.4, 118.2, 55.6, 41.7.

(3d)1-(1H-benzo[d]imidazol-2-yl)-3-methylbutan-1-amine

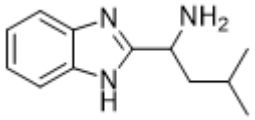

^{1}H NMR (400 MHz, DMSO-d_6): δ 7.60–7.53 (m, 2H, Ar–H), 7.19–7.16 (m, 2H, Ar–H), 4.15 (t, 1H, –CH–NH_2), 2.21 (d, 2H, –CH_2), 1.97 (m, 1H, –$CH(CH_3)_2$), 1.00–0.91 (m, 6H, –CH_3). ^{13}C NMR (100 MHz, DMSO-d_6): δ 158.4, 153.5, 144.2, 139.1, 135.2, 123.5, 118.3, 52.8, 46.7, 25.4, 22.8, 21.6.

(5a)N-(1-(1H-benzo[d]imidazol-2-yl)-2-methylpropyl)-1-(4-isopropylphenyl)methanimine

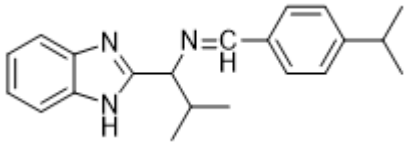

^{1}H NMR (400 MHz, DMSO-d_6): δ 8.65 (s, 1H, –CH=N), 7.82–7.53 (m, 4H, Ar–H), 7.36–7.05 (m, 4H, Ar–H), 5.75 (d, 1H, chiral –CH), 4.12 (m, 1H, –CH), 3.97 (m, 1H, –CH), 1.56 (s, 3H, –CH_3), 1.24 (d, 6H, –$CH(CH_3)_2$). ^{13}C NMR (100 MHz, DMSO-d_6): δ 140.2, 138.5, 132.2, 128.5, 126.4, 122.9, 57.1, 34.3, 22.8, 17.6.

(5b)N-(1-(1H-benzo[d]imidazol-2-yl)ethyl)-1-(4-isopropylphenyl)methanimine

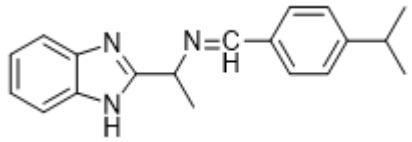

^{1}H NMR (400 MHz, DMSO-d_6): δ 8.65 (s, 1H, –CH=N), 7.82–7.53 (m, 4H, Ar–H), 7.36–7.05 (m, 4H, Ar–), 5.75 (m, 1H, chiral –CH), 4.52 (m, 1H, –CH), 1.56 (s, 3H, $–CH_3$), 1.24 (d, 6H, $–CH(CH_3)_2$). ^{13}C NMR (100 MHz, DMSO-d_6): δ 141.2, 138.9, 133.6, 128.5, 126.4, 125.9, 115.2, 57.1, 34.3, 23.8, 17.6.

(5c)N-(1-(1H-benzo[d]imidazol-2-yl)-2-phenylethyl)-1-(4-isopropylphenyl)methanimine

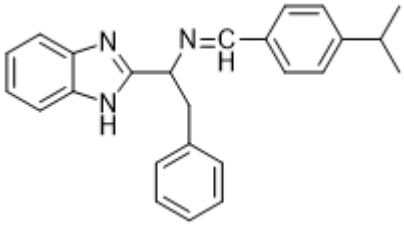

^{1}H NMR (400 MHz, DMSO-d_6): δ 8.65 (s, 1H, –CH=N–), 7.82–7.53 (m, 4H, benzimidazole Ar–H), 7.36–7.05 (m, 4H, Ar–H), 7.23–7.19 (m, 5H, Ar–H), 5.75 (m, 1H, –CH), 3.95 (m, 1H, –CH–NH), 3.95 (d, 2H, $–CH_2$), 1.56 (s, 3H, Ar–CH_3), 1.24 (d, 6H, $–CH(CH_3)_2$). ^{13}C NMR (100 MHz, DMSO-d_6): δ 145.2, 138.9, 133.6, 128.5, 126.4, 125.9, 115.2, 62.8, 46.1, 34.3, 23.8.

(5d) N-(1-(1H-benzo[d]imidazol-2-yl)-3-methylbutyl)-1-(4-isopropylphenyl)methanimine

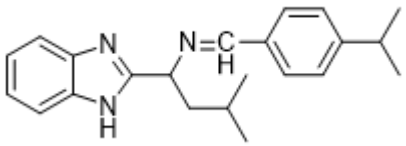

^{1}H NMR (400 MHz, DMSO-d_6): δ 8.65 (s, 1H, –CH=N–), 7.82–7.53 (m, 4H, benzimidazole Ar–H), 7.36–7.05 (m, 4H, Ar–H), 5.75 (t, 1H, –CH=N–CH), 3.95 (m, 1H, –CH), 1.91 (m, 2H, $–CH_2$), 1.75 (m, 1H, –CH), 1.46 (s, 6H, $–CH_3$), 1.24 (d, 6H, $–CH(CH_3)_2$). ^{13}C NMR (100 MHz, DMSO-d_6): δ 141.2, 133.6, 128.5, 126.4, 125.9, 115.2, 57.8, 46.1, 34.3, 23.8.

4. Discussion

All target compounds were analyzed via ^{1}H and ^{13}C NMR spectroscopy using DMSO-d_6 as the solvent. The ^{1}H NMR spectra exhibited aromatic proton signals between δ = 7.00-8.70 ppm, consistent with the expected substitution patterns. Additionally, a distinct singlet around δ = 5.75 ppm was observed, corresponding to the imine (–CH=N–) proton, confirming the formation of the Schiff base linkage. In the ^{13}C NMR spectra, signals associated with aromatic, aliphatic, and imine carbons appeared within their characteristic chemical shift ranges. Specifically, imine carbon atoms were typically found between δ = 140-145 ppm. Collectively, the NMR data substantiated the successful synthesis and structural integrity of the benzimidazole-based Schiff base compounds.

4.1. Theoretical Analysis of Optimized Structures, Frontier Orbital, and Molecular Electrostatic Potential (MEP) Analyses

The molecular geometries of the synthesized Schiff base compounds were fully optimized utilizing the Gaussian 09 computational package. Based on these optimized structures (Figure 3), theoretical analyses such as HOMO-LUMO frontier orbital evaluations and molecular electrostatic potential (MEP) mapping were conducted.

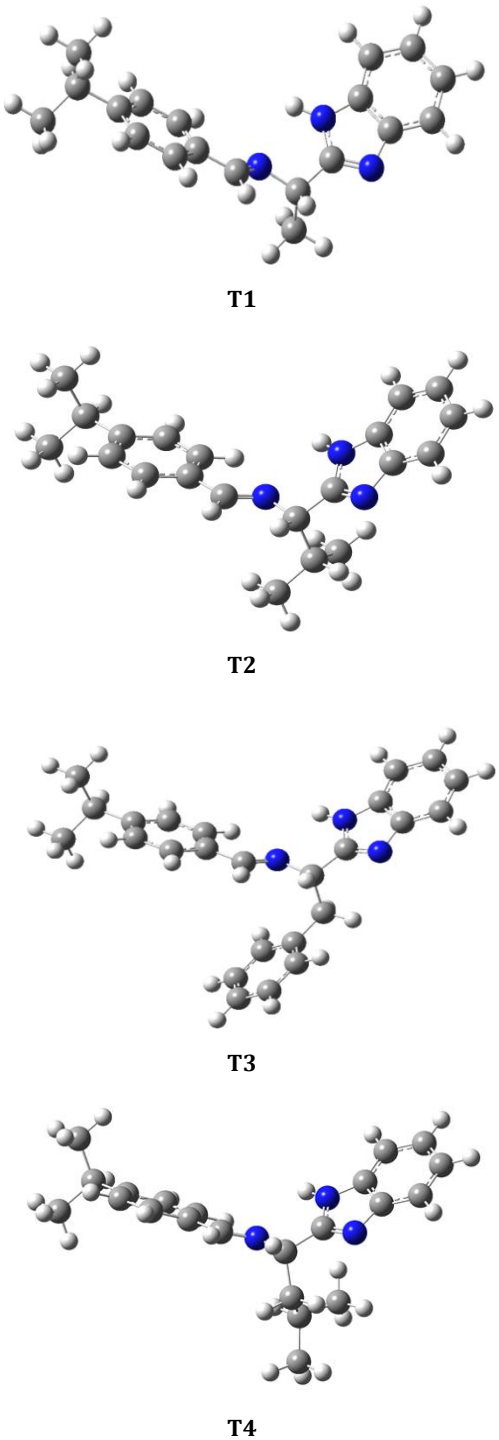

Figure 3. Optimized molecular structures of the synthesized compounds.

These calculations provided valuable information regarding bond distances, angular orientations, and the three-dimensional organization of functional groups, all of which were consistent with experimental observations. Collectively, these theoretical insights contributed to a more comprehensive understanding of the electron distribution patterns and chemical reactivity tendencies of the molecules under investigation.

To understand the charge distribution within the molecules, analyses were performed on the HOMO–LUMO energy levels and Molecular Electrostatic Potential (MEP) surfaces.

In the context of molecular electronic structure, frontier orbitals play a pivotal role in defining a compound's chemical properties and reactivity. These orbitals, commonly known as the HOMO (highest occupied molecular orbital) and LUMO (lowest unoccupied molecular orbital), represent the outermost energy levels involved in electron transitions. The HOMO denotes the uppermost filled orbital, whereas the LUMO indicates the lowest-lying unoccupied orbital, both of which are critical in understanding electron flow during chemical interactions.

One of the most informative parameters for estimating a molecule's electronic characteristics and potential reactivity is the energy difference between its HOMO and LUMO levels. This gap is critically important in elucidating how molecules interact, especially in systems involving reactive intermediates or bioactive compounds. In the field of drug discovery, for instance, interactions between ligands and biological targets are often influenced by the frontier orbitals of the molecules involved. Consequently, theoretical evaluation of HOMO-LUMO energies offers meaningful predictions regarding the compound's chemical nature and potential reactivity. Insights gained from such calculations have broad relevance in diverse research areas including pharmaceutical design, catalysis, and materials science.

For compounds T1-T4, the calculated HOMO energy levels were found to be –5.72, –5.71, –5.73, and –5.70 eV, respectively (Table 1). The LUMO energy levels were determined as –1.45, –1.46, –1.43, and –1.49 eV. The corresponding HOMO–LUMO energy gaps were calculated to be 4.27, 4.24, 4.30, and 4.20 eV, respectively. Among them, compound T4 exhibited the smallest energy gap, indicating that it is the most chemically soft and potentially more stable molecule, suggesting a higher tendency to interact with the target receptor. From a quantum chemical perspective, the molecular interaction mechanism between a ligand and a receptor can be explained by the interaction of the HOMO orbitals on the nucleophilic molecule (e.g., a drug candidate) with the LUMO orbitals on the electrophilic receptor's active site. These interactions play a critical role in initiating chemical reactions and ensuring successful ligand-receptor binding.

To gain deeper insights into the charge distribution and activation mechanisms of the synthesized compounds, Molecular Electrostatic Potential (MEP) maps were computed for each molecule. The MEP surface illustrates the interaction between a hypothetical positive test charge and the molecular surface, thereby providing valuable information about regions of electron density and potential reactive sites.

MEP maps visually express electrostatic interactions across the molecular surface through color gradients. Electron-rich regions, which are potential sites for electrophilic attack, are represented in red. These areas possess high electron density and a strong tendency to donate electrons, making them reactive toward electron-deficient species. In contrast, electron-deficient regions, which are potential sites for nucleophilic attack, appear in blue and are characterized by low electron density and a tendency to attract electrons. This visualization provides crucial insights into the molecule's reactive sites and guides the understanding of its chemical reactivity and interaction potential.

Such electrostatic analyses are instrumental in understanding the chemical reactivity and electronic architecture of molecules. MEP maps are particularly useful in elucidating reaction mechanisms and interaction patterns, offering predictive insight into the nature and strength of chemical bonds (Politzer et al., 2000).

As illustrated in Figure 4, the molecular electrostatic potential (MEP) maps provide valuable insights into the electronic landscape of the studied compounds. The regions exhibiting the most negative potential values, typically ranging between –0.058 and –0.056 a.u., are predominantly concentrated around nitrogen atoms located in the aromatic ring structures. Conversely, the areas of highest positive potential, observed between +0.035 and +0.045 a.u., are associated with N–H functional groups. These electrostatic distributions are instrumental in predicting receptor–ligand interaction hotspots and lay a theoretical foundation for evaluating potential biological activity.

Table 1. HOMO and LUMO orbital representations of the synthesized compounds

	HOMO	LUMO
T1	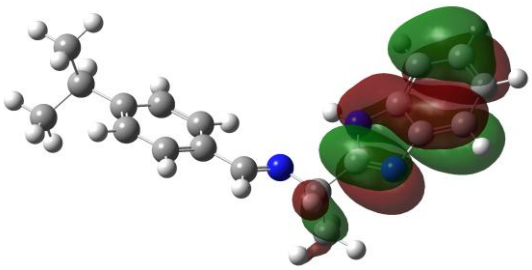	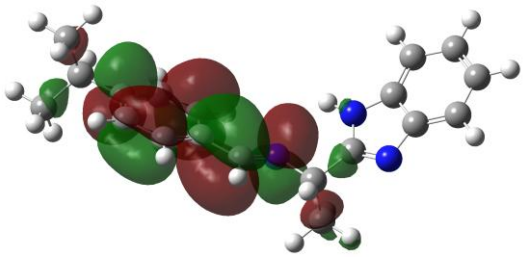
T2	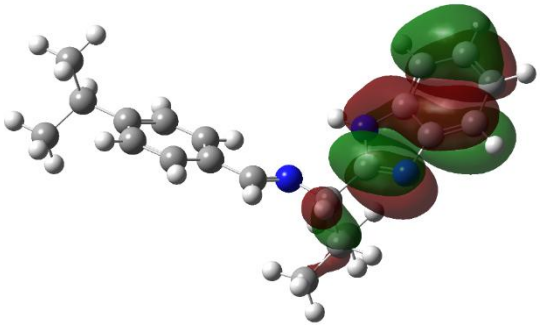	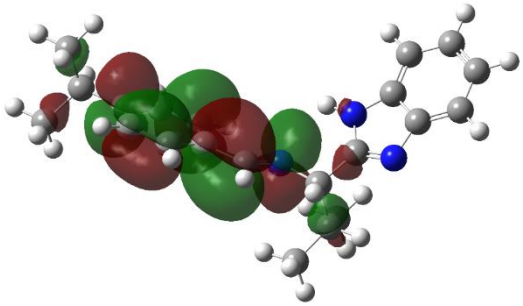
T3	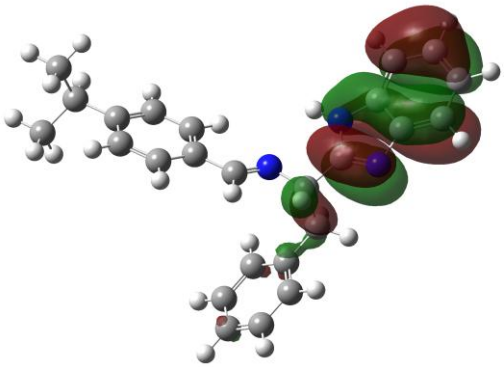	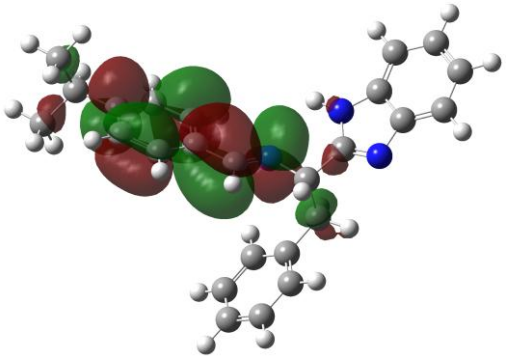
T4	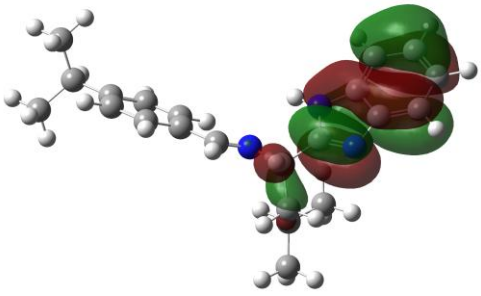	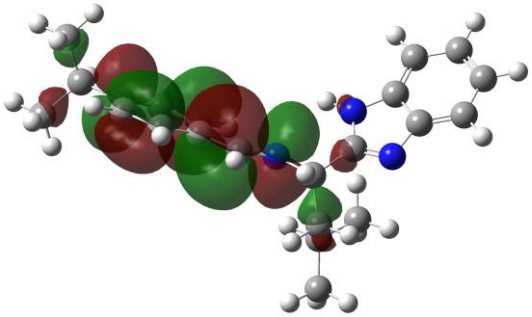

4.2. Structure-Based Docking Studies of Schiff Bases

In this work, molecular docking studies were conducted as part of the computational evaluation of ligand-receptor interactions, a strategy frequently employed in structure-based drug design. This method allows for the prediction of how bioactive compounds spatially orient and bind to specific target proteins. Accordingly, the synthesized Schiff base derivatives were docked to evaluate their potential binding conformations. For this purpose, the crystal structure of the 2WQY protein, known to incorporate the antifungal molecule carboxin (KRB) was obtained from the Protein Data Bank and utilized as the macromolecular target in docking simulations.

The docking simulations provided valuable insights into the binding orientations and interaction profiles of the ligands with the target protein. The docking simulations aimed to identify optimal ligand–receptor binding conformations and assess the therapeutic relevance of the synthesized molecules. Visualization and interpretation of docking outputs were carried out using BIOVIA Discovery Studio Visualizer 2021.

This work represents an important step toward understanding how potential drug molecules bind to

biological targets and supports the identification of promising drug candidates during the early stages of drug development. Molecular docking simulations can serve as a foundational reference for future drug discovery research.

Docking scores are critical parameters that indicate how effectively the ligands interact with the target proteins. Detailed docking scores are presented in Table 2. The binding conformations of the four ligands in the active site of the receptor, as well as the three major types of interactions, are illustrated in Figure 4 in a three-dimensional representation. Visualization of aromatic, hydrogen bond, and hydrophobic interactions between the synthesized compounds and the active site of the receptor is shown in Figure 5. Receptor-KBR ligand interaction analysis is present in Table 3.

Table 2. Docking scores of the synthesized compounds and the natural ligand carboxin (KRB)

Ligantlar	Doking skor (kcal/mol)
KRB	-6.6
T1	-7.2
T2	-6.7
T3	-7.4
T4	-7.5

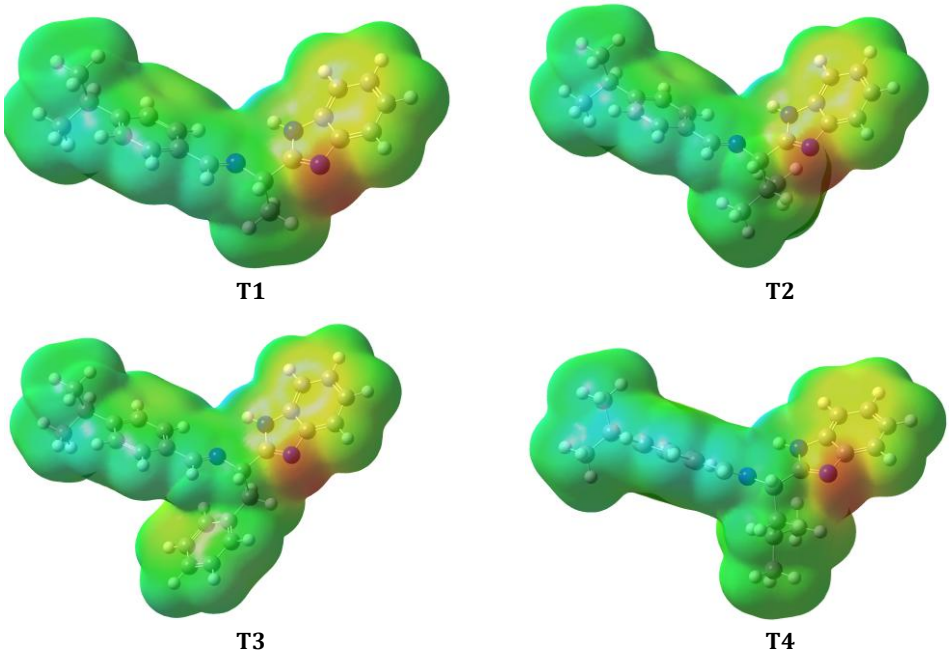

Figure 4. Molecular electrostatic potential (MEP) maps of compounds T1–T4.

Additionally, the binding interactions of the compounds with the receptor structure were systematically examined. Detailed interactions profiles are presented in Tables 4-7, which show the specific atoms of the ligands involved in binding and the modes of interaction with the receptor.

The docking results indicated that compounds T3 and T4 possessed stronger binding affinities than the remaining analogs, as reflected by their more favorable docking scores. This suggests that these two molecules form stronger interactions with the target receptor and may possess greater potential as drug candidates. These findings are significant for evaluating the therapeutic potential of the synthesized ligands in the context of drug design and medicinal research.

Moreover, the molecular docking studies supported these findings by confirming the inhibitory potential of the synthesized compounds. These simulations helped elucidate the interaction patterns between the ligands and the active site residues of the enzyme, offering valuable insights into their possible inhibition mechanisms. Such evaluations play a pivotal role in the rational development of new therapeutic candidates and in enhancing the efficacy of current treatment strategies.

The binding modes of carboxin (KRB) and ligands T1–T4 within the active site of the receptor were stabilized by a variety of non-covalent interactions, including hydrogen bonds, π–π stacking, and hydrophobic contacts such as alkyl and π-alkyl interactions (Figure 6). Additionally, the best affinity values and receptor–ligand interactions are depicted in two-dimensional format in Figures 7–10. Specifically: The KRB ligand formed two classical hydrogen bonds with TRP23 and HIS216 residues. T1 interacted via one hydrogen bond with TRP23. T2 formed four hydrogen bonds involving ARG43, TYR58, and SER39. T4 established two hydrogen bonds with TRP173 and TYR58. T3, by contrast, did not participate in conventional hydrogen bonding; instead, its stabilization within the receptor's binding domain was mediated through electrostatic attractions and hydrophobic contacts.

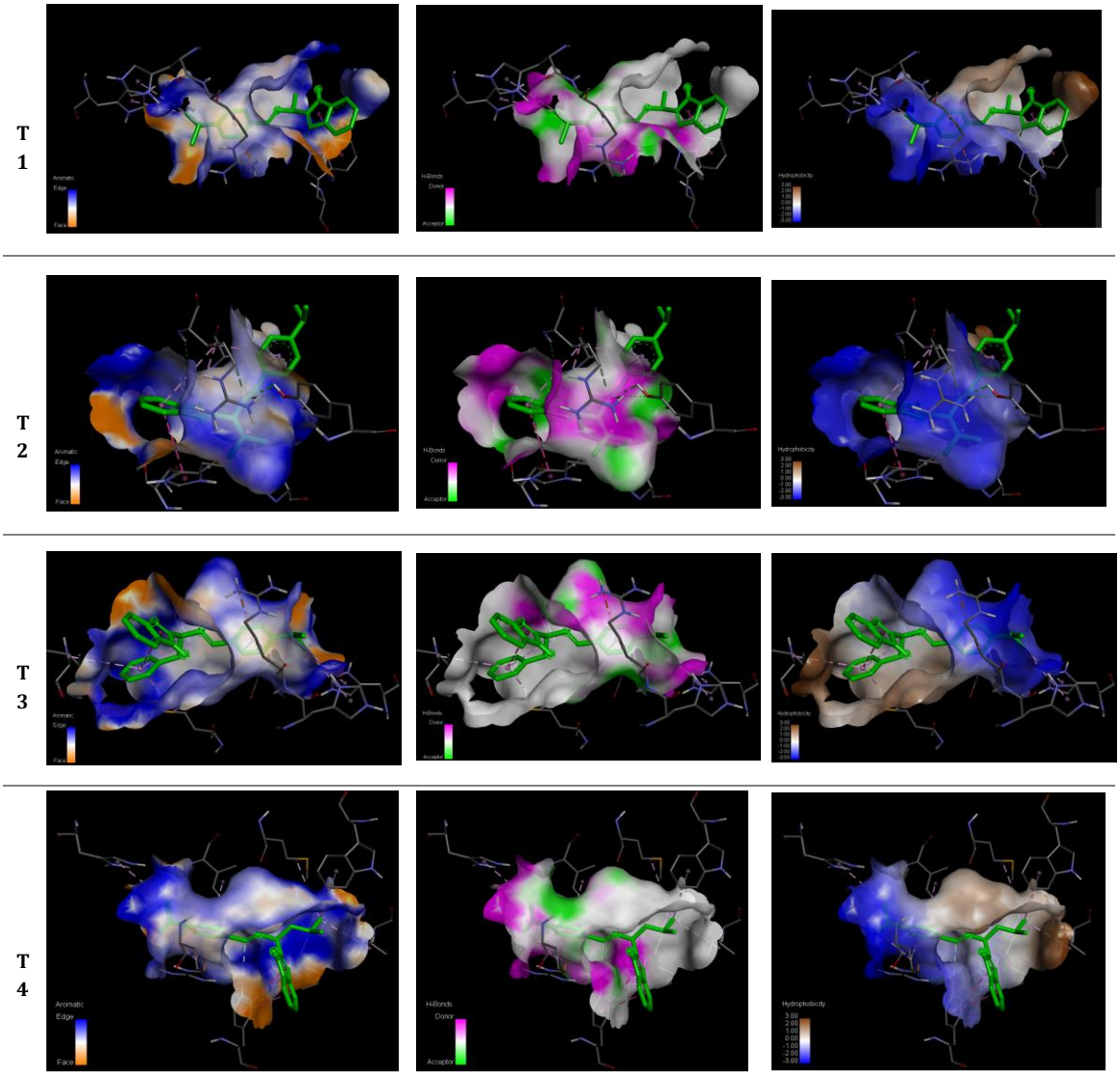

Figure 5. Visualization of aromatic (left), hydrogen bond (middle), and hydrophobic (right) interactions between the synthesized compounds and the active site of the receptor.

Table 3. Receptor-KBR ligand interaction analysis

O:TRP173:HE1 - KBR:O9	1.98168	Hydrogen Bond	Conventional Hydrogen Bond	O:TRP173:HE1	H-Donor	KBR:O9	H-Acceptor	155.317
O:HIS216:CD2 - KBR:O7	3.56057	Hydrogen Bond	Carbon Hydrogen Bond	O:HIS216:CD2	H-Donor	KBR:O7	H-Acceptor	
O:TRP173 - KBR	5.9427	Hydrophobic	Pi-Pi T-shaped	O:TRP173	Pi-Orbitals	KBR	Pi-Orbitals	
P:TRP32 - KBR	5.49439	Hydrophobic	Pi-Pi T-shaped	P:TRP32	Pi-Orbitals	KBR	Pi-Orbitals	
O:ILE218 - KBR	5.05956	Hydrophobic	Alkyl	O:ILE218	Alkyl	KBR	Alkyl	
P:ARG43 - KBR	5.08399	Hydrophobic	Alkyl	P:ARG43	Alkyl	KBR	Alkyl	
KBR - O:PRO169	5.30153	Hydrophobic	Pi-Alkyl	KBR	Pi-Orbitals	O:PRO169	Alkyl	
KBR - P:ILE27	5.49526	Hydrophobic	Pi-Alkyl	KBR	Pi-Orbitals			

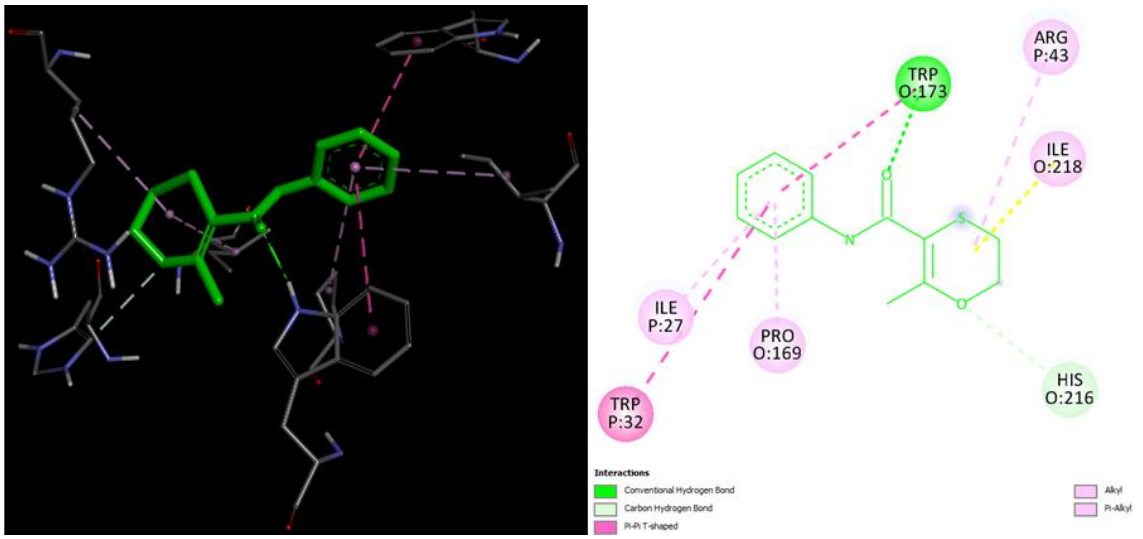

Figure 6. Three-dimensional and two-dimensional interaction diagrams of the KRB compound within the receptor binding site.

Table 4. Receptor–ligand interaction analysis for compound T1

O:TRP173:HE1 - T1:N9	2.4228	Hydrogen Bond	Conventional Hydrogen Bond	O:TRP173:HE1	H-Donor	T1:N9	H-Acceptor	122.518
P:ARG43:NH1 - T1	4.04988	Electrostatic	Pi-Cation	P:ARG43:NH1	Positive	T1	Pi-Orbitals	
T1 - O:TRP173	4.94364	Hydrophobic	Pi-Pi T-shaped	T1	Pi-Orbitals	O:TRP173	Pi-Orbitals	
P:HIS42 - T1:C21	5.32591	Hydrophobic	Pi-Alkyl	P:HIS42	Pi-Orbitals	T1:C21	Alkyl	
P:HIS105 - T1:C21	4.61442	Hydrophobic	Pi-Alkyl	P:HIS105	Pi-Orbitals	T1:C21	Alkyl	
T1 - O:ILE218	5.28524	Hydrophobic	Pi-Alkyl	T1	Pi-Orbitals	O:ILE218	Alkyl	
T1 - P:ARG43	4.63986	Hydrophobic	Pi-Alkyl	T1	Pi-Orbitals	P:ARG43	Alkyl	

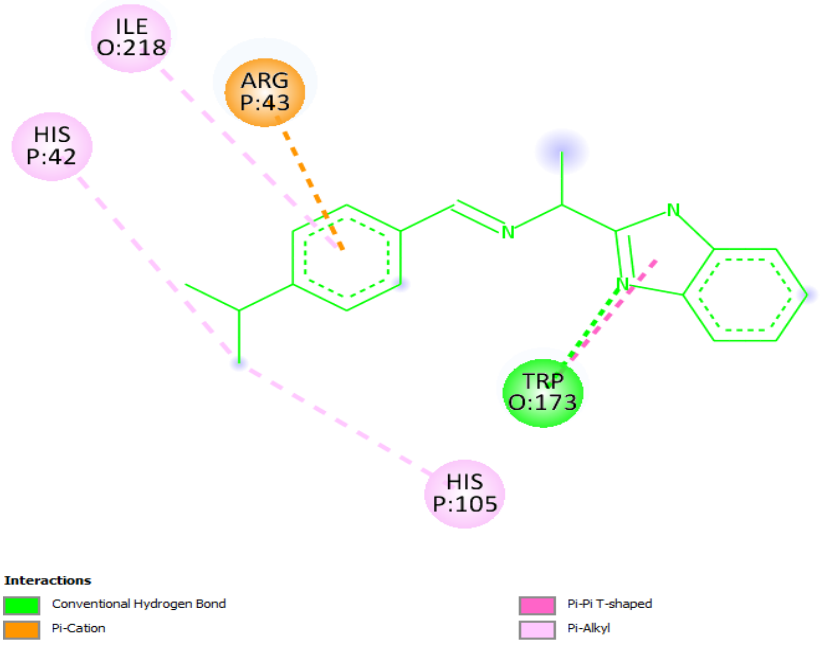

Figure 7. Two-dimensional interaction diagram of the T1 compound within the receptor binding site.

Table 5. Receptor–ligand interaction analysis for compound T2

P:ARG43:HH11 - T2:N11	3.09988	Hydrogen Bond	Conventional Hydrogen Bond	P:ARG43:HH11	H-Donor	T2:N11	H-Acceptor	107.233
Q:TYR58:HH - T2:N11	2.6661	Hydrogen Bond	Conventional Hydrogen Bond	Q:TYR58:HH	H-Donor	T2:N11	H-Acceptor	103.012
T2:H29 - P:SER39:OG	2.09013	Hydrogen Bond	Conventional Hydrogen Bond	T2:H29	H-Donor	P:SER39:OG	H-Acceptor	129.54
P:ARG43:CD - T2:N11	3.35483	Hydrogen Bond	Carbon Hydrogen Bond	P:ARG43:CD	H-Donor	T2:N11	H-Acceptor	121.23
P:ILE40:CG2 - T2	3.8883	Hydrophobic	Pi-Sigma	P:ILE40:CG2	C-H	T2	Pi-Orbitals	
O:HIS216 - T2	5.37473	Hydrophobic	Pi-Pi Stacked	O:HIS216	Pi-Orbitals	T2	Pi-Orbitals	
O:PRO169 - T2	5.38618	Hydrophobic	Alkyl	O:PRO169	Alkyl	T2	Alkyl	
T2 - O:ILE218	5.29224	Hydrophobic	Alkyl	T2	Alkyl	O:ILE218	Alkyl	
T2 - P:ARG43	4.5666	Hydrophobic	Pi-Alkyl	T2	Pi-Orbitals	P:ARG43	Alkyl	
T2 - P:ARG43	5.13274	Hydrophobic	Pi-Alkyl	T2	Pi-Orbitals	P:ARG43	Alkyl	
T2 - P:ARG43	4.93192	Hydrophobic	Pi-Alkyl	T2	Pi-Orbitals	P:ARG43	Alkyl	

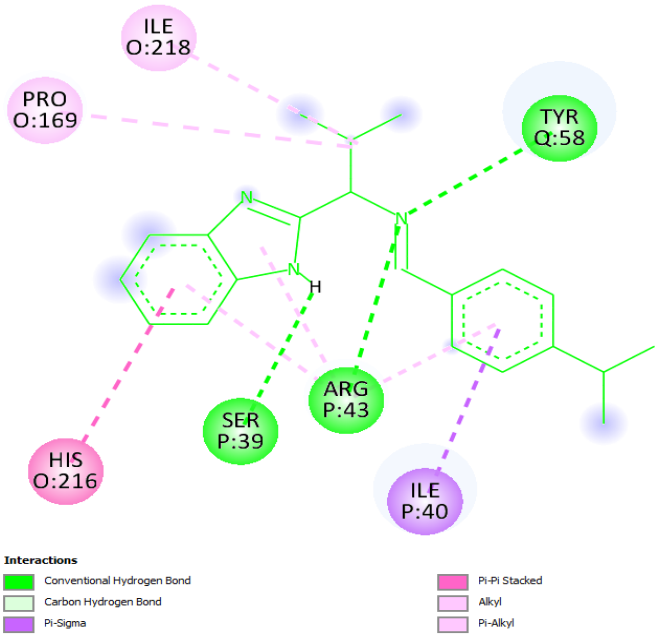

Figure 8. Two-dimensional interaction diagram of the T2 compound within the receptor binding site.

Table 6. Receptor–ligand interaction analysis for compound T3

P:ARG43:NH1 - T3	4.07676	Electrostatic	Pi-Cation	P:ARG43:NH1	Positive	T3	Pi-Orbitals	16.899
T3 - T3	4.37062	Hydrophobic	Pi-Pi T-shaped	T3	Pi-Orbitals	T3	Pi-Orbitals	29.544
P:HIS42 - T3:C22	5.45674	Hydrophobic	Pi-Alkyl	P:HIS42	Pi-Orbitals	T3:C22	Alkyl	
P:HIS105 - T3:C22	4.31398	Hydrophobic	Pi-Alkyl	P:HIS105	Pi-Orbitals	T3:C22	Alkyl	
T3 - O:ILE218	5.45269	Hydrophobic	Pi-Alkyl	T3	Pi-Orbitals	O:ILE218	Alkyl	
T3 - P:ARG43	4.52825	Hydrophobic	Pi-Alkyl	T3	Pi-Orbitals	P:ARG43	Alkyl	
T3 -	5.38562	Hydrophobic	Pi-Alkyl	T3	Pi-Orbitals	O:PRO169	Alkyl	
T3 - P:ILE27	4.99901	Hydrophobic	Pi-Alkyl	T3	Pi-Orbitals	P:ILE27	Alkyl	
T3 - P:MET36	5.40581	Hydrophobic	Pi-Alkyl	T3	Pi-Orbitals	P:MET36	Alkyl	

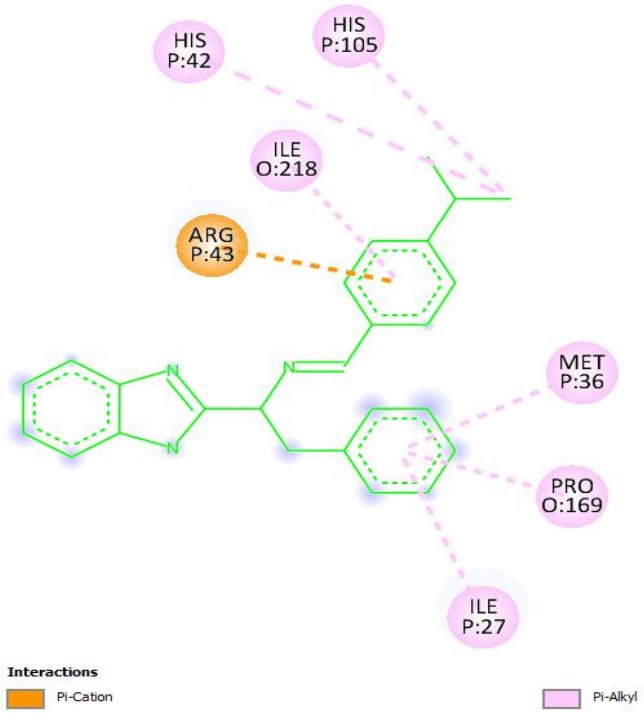

Figure 9. Two-dimensional interaction diagram of the T3 compound within the receptor binding site.

Table 7. Receptor–ligand interaction analysis for compound T4

O:TRP173:HE1 - T4:N9	2.68725	Hydrogen Bond	Conventional Hydrogen Bond	O:TRP173:HE1	H-Donor	T4:N9	H-Acceptor	110.156
T4:C13 - Q:TYR58:OH	3.20641	Hydrogen Bond	Carbon Hydrogen Bond	T4:C13	H-Donor	Q:TYR58:OH	H-Acceptor	131.18
P:ARG43:NH1 - T4	3.90114	Electrostatic	Pi-Cation	P:ARG43:NH1	Positive	T4	Pi-Orbitals	
Q:TYR58 - T4	4.3497	Hydrophobic	Pi-Pi Stacked	Q:TYR58	Pi-Orbitals	T4	Pi-Orbitals	
T4 - Q:TYR58	4.79674	Hydrophobic	Pi-Pi Stacked	T4	Pi-Orbitals	Q:TYR58	Pi-Orbitals	
T4:C21 - P:ARG43	4.02215	Hydrophobic	Alkyl	T4:C21	Alkyl	P:ARG43	Alkyl	
T4:C24 - P:ILE27	4.49216	Hydrophobic	Alkyl	T4:C24	Alkyl	P:ILE27	Alkyl	
T4:C24 - P:MET36	5.28682	Hydrophobic	Alkyl	T4:C24	Alkyl	P:MET36	Alkyl	
O:TRP172 - T4:C24	5.03417	Hydrophobic	Pi-Alkyl	O:TRP172	Pi-Orbitals	T4:C24	Alkyl	
P:TRP32 - T4:C24	5.1873	Hydrophobic	Pi-Alkyl	P:TRP32	Pi-Orbitals	T4:C24	Alkyl	
P:HIS105 - T4:C22	4.65182	Hydrophobic	Pi-Alkyl	P:HIS105	Pi-Orbitals	T4:C22	Alkyl	
T4 - O:ILE218	5.30821	Hydrophobic	Pi-Alkyl	T4	Pi-Orbitals	O:ILE218	Alkyl	
T4 - P:ARG43	4.69995	Hydrophobic	Pi-Alkyl	T4	Pi-Orbitals	P:ARG43	Alkyl	

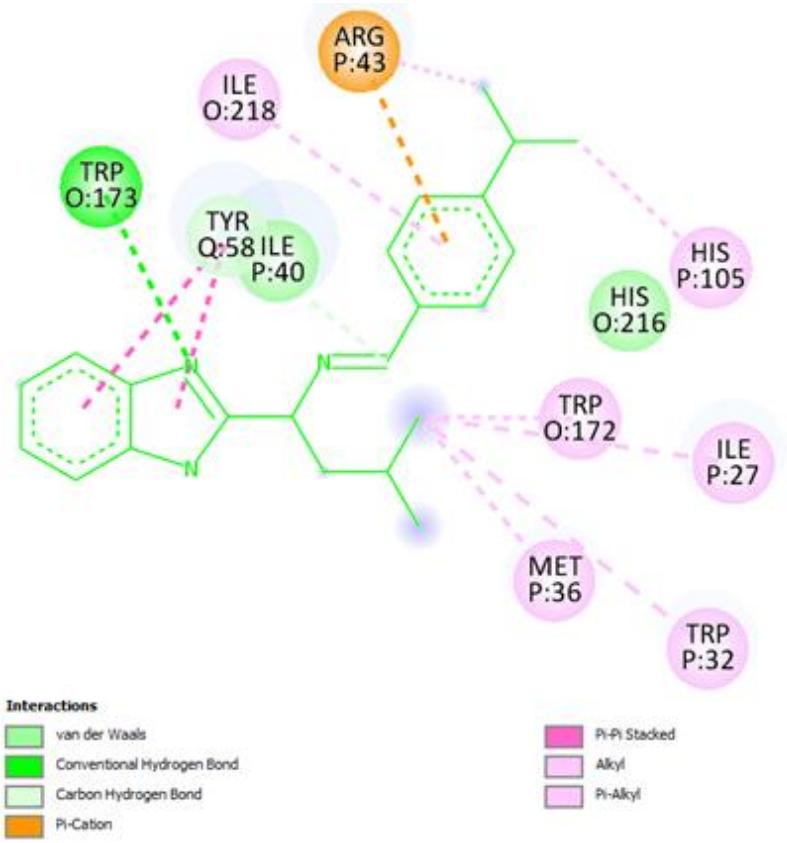

Figure 10. Two-dimensional interaction diagram of the T4 compound within the receptor binding site.

These interactions enable the ligands to bind selectively and specifically to the receptor, which in turn may influence their biological activity. Hydrogen bonds occur between electronegative atoms (such as O and N) on the ligand and hydrogen-bond-forming residues on the receptor, facilitating tighter binding and potentially enhancing activity. Meanwhile, hydrophobic interactions, such as alkyl and π-alkyl contacts, stabilize the ligand within hydrophobic regions of the receptor, contributing to binding affinity. Such interaction analyses are vital for understanding drug–target interactions, as a detailed knowledge of receptor–ligand binding can guide the design of more effective therapeutic molecules.

5. Conclusions

Within the scope of this project, benzimidazole derivatives which play a significant role in pharmaceutical chemistry were successfully synthesized and reacted with 4-(dimethylamino)benzaldehyde to obtain Schiff bases. Alongside their synthesis, the ligands were subjected to geometry optimization via Density Functional Theory (DFT), followed by molecular docking analyses to explore their potential bioactivity.

To investigate the potential interaction profiles of the synthesized compounds, molecular docking analyses were carried out to assess their possible binding orientations and conformational preferences. As a result, all four Schiff bases demonstrated potential as inhibitors against the 2WQY protein structure, with two of them showing particularly strong binding affinities, indicating a higher likelihood of biological effectiveness.

When evaluated in conjunction with biological activity predictions, the molecular docking results suggest that all synthesized compounds possess promising bioactive profiles and may serve as potential drug candidates. Owing to their demonstrated bioactivity, these benzimidazole-based Schiff bases offer a strong foundation for future research and development. Moreover, the synthesized molecules not only show potential as pharmaceutical precursors but may also act as effective ligands in coordination chemistry involving transition metal ions.

Author Contributions

The percentages of the author' contributions are presented below. The author reviewed and approved the final version of the manuscript.

	N.T.S.
C	100
D	100
S	100
DCP	100
DAI	100
L	100
W	100
CR	100
SR	100
PM	100
FA	100

C=Concept, D= design, S= supervision, DCP= data collection and/or processing, DAI= data analysis and/or interpretation, L= literature search, W= writing, CR= critical review, SR= submission and revision, PM= project management, FA= funding acquisition.

Conflict of Interest

The author declared that there is no conflict of interest.

Ethical Consideration

No ethics committee approval was obtained for this research as no studies were conducted on animals or humans.

Acknowledgement

I would like to thank the Scientific Research Projects Coordination Unit of Kırşehir Ahi Evran University for supporting this study under the project number MMF.A4.23.007. Additionally, I would like to express my deep gratitude to Assoc. Prof. Tuncay Karakurt for his invaluable help and contributions to the theoretical calculations of this research.

References

Ashraf, M., Wajid, A., Mahmood, K., Maah, M. J., & Yusoff, I. B. (2011). Spectral investigation of the activities of amino substituted bases. *Oriental Journal of Chemistry, 27*(1), 363–372.

Asif, M. (2019). Green synthesis of benzimidazole derivatives: an overview on green chemistry and its applications. *Chemical Methodology, 3*(6), 620–631. https://doi.org/10.33945/SAMI/CHEMM.2019.6.1

Aydınlı, E. A. (2006). *Antimicrobial effects of some Schiff bases* (Yüksek lisans tezi, Ankara Üniversitesi, Fen Bilimleri Enstitüsü).

Becke, A. D. (1993). Density-functional thermochemistry. III. The role of exact exchange. *The Journal of Chemical Physics, 98*(7), 5648–5652.

Chang, Y. S. (2012). Hypersensitivity reactions to proton pump inhibitors. *Current Opinion in Allergy and Clinical Immunology, 12*(4), 348–353.

Dallakyan, S., & Olson, A. J. (2015). Small-molecule library screening by docking with PyRx. In J. Hempel, C. Williams, & C. Hong (Eds.), *Chemical Biology Methods in Molecular Biology* (Vol. 1263, pp. 243–250). Humana Press. https://doi.org/10.1007/978-1-4939-2269-7_19

Dennington, R., Keith, T., & Millam, J. (2009). *GaussView, version 5*. Semichem Inc.

DiRisio, R. J., Armstrong, J. E., Frank, M. A., Lake, W. R., & McNamara, W. R. (2017). Cobalt Schiff-base complexes for electrocatalytic hydrogen generation. *Dalton Transactions, 46*(32), 10418–10425.

Emregül, K. C., Düzgün, E., & Atakol, O. (2006). The application of some polydentate Schiff base compounds containing aminic nitrogens as corrosion inhibitors for mild steel in acidic media. *Corrosion Science, 48*(10), 3243–3260.

Foresman, J. B., & Frisch, A. (1996). *Exploring chemistry with electronic structure methods: a guide to using Gaussian* (2nd ed.). Gaussian Inc.

Frisch M, Trucks G, Schlegel HB, Scuseria G, Robb M, Cheeseman J, Scalmani G, Barone V, Mennucci B, Petersson G. 2009. Gaussian 09, revision A.02, Gaussian Inc, Wallingford, CT, USA, pp: 200.

Golcu, A., Tümer, M., Demirelli, H., & Wheatley, R. (2005). Cd(II) and Cu(II) complexes of polydentate Schiff base ligands: synthesis, characterization, properties and biological activity. *Inorganica Chimica Acta, 358*(6), 1785–1797.

Iwamoto, K., Uehara, Y., Inoue, Y., Taguchi, K., Muraoka, D., Ogo, N., Matsuno, K., & Asai, A. (2017). Inhibition of STAT3 by anticancer drug bendamustine. *PLoS One, 12*(1), Article e0169123.

Lasri, J., Elsherbiny, A. S., Eltayeb, N. E., Haukka, M., & El-Hefnawy, M. E. (2018). Synthesis and characterization of ferrocene-based Schiff base and ferrocenecarboxaldehyde oxime and their adsorptive removal of methyl blue from aqueous solution. *Journal of Organometallic Chemistry, 866*, 21–26.

Lee, C., Yang, W., & Parr, R. G. (1988). Development of the Colle-Salvetti correlation-energy formula into a functional of the electron density. *Physical Review B, 37*(2), 785–789.

Lieberman, L. A., & Higgins, D. E. (2009). A small molecule screen identifies the antipsychotic drug pimozide as an inhibitor of *Listeria monocytogenes* infection. *Antimicrobial Agents and Chemotherapy, 53*(2), 756–764.

Pfeiffer, P., Breith, E., Lübbe, E., & Tsumaki, T. (1932). Thcylische orthokondesierte Nebenvalenzringe. *Annalen der Chemie, 492*(1), 81–127.

Politzer, P., Concha, M. C., & Murray, J. S. (2000). Density functional study of dimers of dimethylnitramine. *International Journal of Quantum Chemistry, 80*(2), 184–192.

Redshaw, C. (2017). Use of Metal Catalysts Bearing Schiff Base Macrocycles for the Ring Opening Polymerization (ROP) of Cyclic Esters. *Catalysts, 7*(5), 165.

Rehman, W., Baloch, M. K., Muhammad, B., Badshah, A., & Khan, K. M. (2004). Characteristic spectral studies and in vitro antifungal activity of some Schiff bases and their organotin (IV) complexes. *Chinese Science Bulletin, 49*(2), 119–122.

Schiff, H. (1869). Untersuchungen Uber Salicin Derivate. *European Journal of Organic Chemistry, 150*(3), 193–200.

Silva da, C. M., Silva da, D. L., Modolo, L. V., & Alves, R. B. (2011). Schiff bases: a short review of their antimicrobial activities. *Journal of Advanced Research, 2*(1), 1–8.

Upadhyay, K. K., Kumar, A., Upadhyay, S., & Mishra, P. C. (2008). Synthesis, characterization, structural optimization using density functional theory and superoxide ion scavenging

activity of some Schiff bases. *Journal of Molecular Structure, 873*(1–3), 5–16.

Vigato, P. A., & Tamburini, S. (2004). The Challenge of Cyclic and Acyclic Schiff Bases and Related Derivatives. *Coordination Chemistry Reviews, 248*(17–20), 1717–2128.

Yeap, G. Y., Ha, S. T., Ishizawa, N., Suda, K., Boey, P. L., & Mahmood, W. A. K. (2003). Synthesis, crystal structure and spectroscopic study of para substituted 2-hydroxy-3-methoxybenzalideneanilines. *Journal of Molecular Structure, 658*(1–3), 87–99.

Zeishen, W., Zigi, G., & Zhenhuan, Y. (1990). Synthesis, characterization and anticanser activity of L-alanine Schiff base complexes of copper(II), zinc(II), and cobalt (II). *Synthetic Reactivity in Inorganic and Metal-Organic Chemistry, 20*(3), 335–344.

Zhang, J., Xu, L., & Wong, W. Y. (2018). Energy materials based on metal Schiff base complexes. *Coordination Chemistry Reviews, 355*, 180–198.

Zhang, P., Wang, H., Sun, L., Zhang, J., Xi, Y., Wu, Y., Yan, L. L., Li, X., & Sun, N. (2017). Telmisartan and hydrochlorothiazide antihypertensive treatmentin high sodium intake population: A randomized double blind trial. *Journal of Hypertension, 35*(10), 2077–2085.